

Quasi-integrability and nonlinear resonances in cold atoms under modulation

Gupta, Rahul; Jain, Manan; Jain, Sudhir R.

DOI:

[10.1098/rsos.231503](https://doi.org/10.1098/rsos.231503)

License:

Creative Commons: Attribution (CC BY)

Document Version

Publisher's PDF, also known as Version of record

Citation for published version (Harvard):

Gupta, R, Jain, M & Jain, SR 2024, 'Quasi-integrability and nonlinear resonances in cold atoms under modulation', *Royal Society Open Science*, vol. 11, no. 4, 231503. <https://doi.org/10.1098/rsos.231503>

[Link to publication on Research at Birmingham portal](#)

General rights

Unless a licence is specified above, all rights (including copyright and moral rights) in this document are retained by the authors and/or the copyright holders. The express permission of the copyright holder must be obtained for any use of this material other than for purposes permitted by law.

- Users may freely distribute the URL that is used to identify this publication.
- Users may download and/or print one copy of the publication from the University of Birmingham research portal for the purpose of private study or non-commercial research.
- User may use extracts from the document in line with the concept of 'fair dealing' under the Copyright, Designs and Patents Act 1988 (?)
- Users may not further distribute the material nor use it for the purposes of commercial gain.

Where a licence is displayed above, please note the terms and conditions of the licence govern your use of this document.

When citing, please reference the published version.

Take down policy

While the University of Birmingham exercises care and attention in making items available there are rare occasions when an item has been uploaded in error or has been deemed to be commercially or otherwise sensitive.

If you believe that this is the case for this document, please contact UBIRA@lists.bham.ac.uk providing details and we will remove access to the work immediately and investigate.



Research

Cite this article: Gupta R, Jain M, Jain SR. 2024 Quasi-integrability and nonlinear resonances in cold atoms under modulation. *R. Soc. Open Sci.* **11:** 231503.
<https://doi.org/10.1098/rsos.231503>

Received: 3 October 2023

Accepted: 20 February 2024

Subject Category:

Physics and biophysics

Subject Areas:

atomic and molecular physics, quantum physics

Keywords:

ultracold atoms, quasi-integrability, semiclassical methods, quantum chaos, dynamical localization

Author for correspondence:

Manan Jain

e-mail: m.jain@bham.ac.uk

Quasi-integrability and nonlinear resonances in cold atoms under modulation

Rahul Gupta¹, Manan Jain² and Sudhir R. Jain³

¹Department of Physics, Indian Institute of Technology, Mumbai 400076, India

²School of Physics and Astronomy, University of Birmingham, Birmingham B15 2TT, UK

³UM-DAE Centre for Excellence in Basic Sciences, University of Mumbai, Vidyanageri Campus, Mumbai 400098, India

MJ, 0000-0003-3693-7738

Quantum dynamics of a collection of atoms subjected to phase modulation has been carefully revisited. We present an exact analysis of the evolution of a two-level system (represented by a spinor) under the action of a time-dependent matrix Hamiltonian. The dynamics is shown to evolve on two coupled potential energy surfaces (PESs): one of them is binding, while the other one is scattering type. The dynamics is shown to be quasi-integrable with nonlinear resonances. The bounded dynamics with intermittent scattering at random moments presents a scenario reminiscent of Anderson and dynamical localization. We believe that a careful analytical investigation of a multi-component system that is classically non-integrable is relevant to many other fields, including quantum computation with multi-qubit systems.

1. Introduction

Evolution in the fields of ultracold atoms and quantum physics in the past few decades has led to the recognition of these fields as a huge well-acclaimed arena for the exploration of popular subjects like quantum chaos [1], Feshbach resonances [2–12], ultracold atomic mixtures [13–18], atom interferometry [19–33], atomic clocks [34–44], quantum diffraction [45,46] and quantum thermodynamics [47–50]. This is due to the rich internal structures, longer de Broglie wavelengths and tunable long-range interactions of ultracold atoms. Furthermore, the research in the regime of lower temperatures has also been extended to these molecules [51,52]. Apart from these recent developments, there has been a sustained effort to realize parallels between atomic and condensed matter physics [53]. One of the ideas pursued with great interest is the localization of states in disordered systems, pioneered by Anderson [54]. Due to a common-sense analogy between disorder and

chaos, a connection between the localization of wavefunctions of classically chaotic systems and the disordered lattices of infinite [55] and finite extent [56] was brought out. Even in matter waves, the phenomenon of localization has been experimentally demonstrated [57].

Many years ago, an experiment carried out by the group led by Raizen [1] demonstrated the dynamical analogue of Anderson localization in a system of cold atoms. In this experiment, approximately 100 000 ^{23}Na atoms were trapped in a spherical volume of radius 300 μm at a temperature of 17 μK . At the end of the preparation step, the cooling lasers were turned off and a modulated standing light field was switched on for 10 μs . The Hamiltonian describing the interaction of a sodium atom of mass m at position x and momentum p with the light field is given by [58]

$$H_0 = H_{\text{el}} + \frac{p^2}{2m} + eF \cos\{k_L[x - \Delta L \sin \omega t]\} \cos \omega_L t. \quad (1.1)$$

Here, H_{el} denotes the interaction of valence electrons with an atom. The last term denotes the electric dipole interaction of the electromagnetic field with an electron. The laser frequency and wavenumber are denoted by ω_L and k_L , respectively, and ω is the modulation frequency. Standing waves are generated by directing two counter-propagating laser beams into the trap and the modulation is achieved by passing one beam through an electro-optical phase modulator. The beam is made to strike a mirror in a cavity of length ΔL that is moving with the modulation frequency, ω . The laser frequency was chosen close to the D_2 line of sodium. The electronic Hamiltonian can be reduced to a two-level system written on the basis of a ground state $|g\rangle = (0, 1)^T$ and an excited state, $|e\rangle = (1, 0)^T$, such that a general state with complex amplitudes ψ^+ and ψ^- in the respective two levels can be written as $\psi = \psi^+ |e\rangle + \psi^- |g\rangle$. Taking the energy average of the two states as zero energy, the matrix elements of H_{el} and eF together give

$$H_{\text{el}} = \frac{\hbar\omega_0}{2} \sigma_z; \quad eF = \hbar\Omega \sigma_x \implies H_{\text{el}} + eF = \begin{pmatrix} \hbar\omega_0/2 & \hbar\Omega \\ \hbar\Omega & -\hbar\omega_0/2 \end{pmatrix} \quad (1.2)$$

where the transition frequency between these two levels is denoted by ω_0 , Ω denotes the Rabi frequency coupling the two states by electric dipole interaction and σ 's are the Pauli matrices. Thus, H_0 may be written as

$$H_0 = \frac{p^2}{2m} \mathbf{I} + \frac{\hbar\omega_0}{2} \sigma_z + \hbar\Omega \cos\{k_L[x - \Delta L \sin \omega t]\} \cos(\omega_L t) \sigma_x \quad (1.3)$$

where \mathbf{I} denotes an identity matrix.

After we present the general Hamiltonian below, in §2, we present the Hamiltonian under rotating wave approximation (RWA). Within this approximation, the case of adiabatic perturbation for the two cases of small and large detuning is considered. In §3, the exact solution for this matrix Hamiltonian is given. The method transforms the dynamics under the matrix Hamiltonian to dynamics on potential energy surfaces (PESs). Classical dynamics reveals the presence of nonlinear resonances in §4. The classical system obeys the Kolmogorov–Arnold–Moser (KAM) theorem [59] and hence is quasi-integrable [60]. In a related context of the quantum Rabi model, a discussion on integrability [61] and symmetries [62] has been presented relatively recently.

Special solutions are discussed as they have been used to analyse experiments carried out by different groups. For each case discussed at the quantum mechanical level, we also present classical phase space pictures and show that this atomic system presents a very interesting and deep instance of the association of quasi-integrability and dynamical localization. The phase space pictures exhibit certain misleading features in the approximated Hamiltonian, compared with the exact Hamiltonian obtained by systematic expansion in powers of \hbar .

1.1. General Hamiltonian

We now transform to a frame which is rotating with ω_L about the z-axis in a spin space,

$$\psi_{\text{rot}} = \exp(i\omega_L \sigma_z t / 2) \psi. \quad (1.4)$$

Substituting ψ in the Schrödinger equation, $i\hbar \partial \psi / \partial t = H_0 \psi$, we have the equation for the rotated wavefunction,

$$H_{\text{rot}} = \frac{p^2}{2m} \mathbf{I} + \frac{\hbar(\omega_0 - \omega_L)}{2} \sigma_z + \hbar\Omega \cos \{k_L[x - \Delta L \sin \omega t]\} \times \cos(\omega_L t) e^{i\omega_L \sigma_z t/2} \sigma_x e^{-i\omega_L \sigma_z t/2}. \quad (1.5)$$

Using the standard identity, $e^{i\omega_L \sigma_z t/2} \sigma_x e^{-i\omega_L \sigma_z t/2} = \sigma_x \cos \omega_L t - \sigma_y \sin \omega_L t$, we have the transformed Hamiltonian,

$$H_{\text{rot}} = \frac{p^2}{2m} \mathbf{I} + \frac{\hbar(\omega_0 - \omega_L)}{2} \sigma_z + \frac{\hbar\Omega}{2} \cos \{k_L[x - \Delta L \sin \omega t]\} \times [\sigma_x(1 + \cos 2\omega_L t) - \sigma_y \sin 2\omega_L t]. \quad (1.6)$$

This is the general Hamiltonian for the physical situation described above where there are terms oscillating with twice the ω_L .

2. Rotating wave approximation

The Schrödinger equation for H_{rot} is usually solved under the RWA [58,63]. Here, the terms oscillating with frequency $2\omega_L$ are neglected. This leads to a simplified Hamiltonian,

$$H_{\text{rot}}^{\text{RWA}} = \frac{p^2}{2m} \mathbf{I} + \hbar\Omega_{\text{eff}}(\sigma_z \cos \alpha + \sigma_x \sin \alpha), \quad (2.1)$$

where

$$\Omega_{\text{eff}} = \frac{1}{2} [(\omega_0 - \omega_L)^2 + \Omega^2 \cos^2 \{k_L(x - \Delta L \sin \omega t)\}]^{1/2}, \quad (2.2)$$

$$\tan \alpha = \frac{\Omega \cos \{k_L(x - \Delta L \sin \omega t)\}}{\omega_0 - \omega_L}.$$

Let us rotate the state of this Hamiltonian further in the spin space by an angle $(-\alpha/2)$ about the y -axis, to obtain a new state, $\psi' = \psi'^+ |e\rangle + \psi'^- |g\rangle = \exp(i\alpha\sigma_y/2)\psi_{\text{rot}}$

$$\psi' = \begin{pmatrix} \cos(\alpha/2) e^{i\omega_L t/2} \psi^+ + \sin(\alpha/2) e^{-i\omega_L t/2} \psi^- \\ -\sin(\alpha/2) e^{i\omega_L t/2} \psi^+ + \cos(\alpha/2) e^{-i\omega_L t/2} \psi^- \end{pmatrix} \quad (2.3)$$

in which the second term is diagonal. Consequently, the equation satisfied by ψ' is

$$i\hbar \frac{\partial \psi'}{\partial t} = -\frac{\hbar}{2} \frac{\partial \alpha}{\partial t} \sigma_y \psi' + e^{i\alpha\sigma_y/2} H_{\text{rot}}^{\text{RWA}} e^{-i\alpha\sigma_y/2} \psi' = H_{\text{eff}}^{\text{RWA}} \psi'. \quad (2.4)$$

However, this will transform the kinetic term as [64]

$$e^{i\alpha\sigma_y/2} p^2 \mathbf{I} e^{-i\alpha\sigma_y/2} \psi' = (\mathbf{pI} - \hbar\mathbf{A})^2 \psi' = \mathbf{\Pi}^2 \psi', \quad (2.5)$$

$$\mathbf{A} = \frac{\sigma_y}{2} \frac{\partial \alpha}{\partial x} = \frac{-k_L \delta_L \Omega \sin \{k_L(x - \Delta L \sin \omega t)\} \sigma_y}{2(\delta_L^2 + \Omega^2 \cos^2 \{k_L(x - \Delta L \sin \omega t)\})}. \quad (2.6)$$

where \mathbf{I} is an identity matrix. Now, we can use the well-known identity

$$e^{i\alpha(\hat{n} \cdot \vec{\sigma})} \vec{\sigma} e^{-i\alpha(\hat{n} \cdot \vec{\sigma})} = \vec{\sigma} \cos 2\alpha + \hat{n} \times \vec{\sigma} \sin 2\alpha + \hat{n}(\hat{n} \cdot \vec{\sigma})(1 - \cos 2\alpha). \quad (2.7)$$

While the 'potential' part of the Hamiltonian becomes diagonal with these unitary transformations, the kinetic term modifies to $(\mathbf{pI} - \hbar\mathbf{A})^2$. This has terms of order 1, \hbar and \hbar^2 ; thus, an asymptotic semiclassical expansion appears in a natural manner [65–67]. The asymptotic expansion parameter \hbar [64] is small compared with the relevant classical action.¹ It is worth noting that this powerful method has been successfully used to obtain the 'exact' ground states for deuteron [68] and triton [69]. Moreover, we would like to recall that the semiclassical trace formula for oscillator potentials gives

¹We can make a rough estimate of relevant classical action by considering the product of momentum of the trapped sodium atom and the size of the trap. With the values corresponding to the experiment [1]. The momentum corresponding to 17 μK is approximately $4.23 \times 10^{-27} \text{ kg m s}^{-1}$. In a spherical trap of radius, 300 μm , the ratio of \hbar to the action is estimated to be about 10^{-5} . If the atom remains in a smaller region, this ratio would still be at least 10^{-4} or so. A semiclassical expansion is certainly justified.

the exact level density, where one performs an asymptotic expansion of the energy-dependent Green function or propagator in powers of \hbar [70].

Furthermore, since \mathbf{A} has non-zero diagonal matrix elements, there is a possibility of a geometric phase appearing in the state of the atoms as the system evolves. This is indeed due to the cavity modulation. Dimensionally, $\hbar\mathbf{A}/e$ is a magnetic vector potential. $H_{\text{eff}}^{\text{RWA}}$ can be written as

$$H_{\text{eff}}^{\text{RWA}} = \frac{\Pi^2}{2m} + \hbar\Omega_{\text{eff}}\sigma_z - \frac{\hbar}{2} \frac{\partial\alpha}{\partial t} \sigma_y, \quad (2.8)$$

$$= \left[\frac{p^2}{2m} + \frac{\hbar^2}{8m} \left(\frac{\partial\alpha}{\partial x} \right)^2 \right] \mathbf{I} + \hbar\Omega_{\text{eff}}\sigma_z + \left(-\frac{\hbar}{2} \frac{\partial\alpha}{\partial t} - \frac{\hbar}{2} \frac{\partial\alpha}{\partial x} \frac{p}{m} + \frac{i\hbar^2}{2m} \frac{\partial\alpha}{\partial x} \right) \sigma_y. \quad (2.9)$$

Except for terms of order $O(\hbar^2)$, each of the terms can make a significant contribution. At this point, one of the possible simplifications occurs if α is slowly varying with time. This leads us to consider applying the adiabatic approximation, which we will discuss now.

2.1. Adiabatic variation

We may neglect the term $\hbar\sigma_y d\alpha/dt$. Here, we invoke the classical correspondence of dx/dt and \mathbf{p}/m by writing²

$$\hbar\sigma_y \frac{d\alpha}{dt} \rightarrow \hbar \frac{\partial\alpha}{\partial x} \frac{p}{m} \sigma_y + \hbar \frac{\partial\alpha}{\partial t} \sigma_y, \quad (2.10)$$

which is small for an adiabatic variation. The adiabatic Hamiltonian is

$$H_{\text{ad}}^{\text{RWA}} = \frac{1}{2m} \left[p^2 + \frac{\hbar^2}{8m} \left(\frac{\partial\alpha}{\partial x} \right)^2 \right] \mathbf{I} + \hbar\Omega_{\text{eff}}\sigma_z + \frac{i\hbar^2}{2m} \frac{\partial\alpha}{\partial x} \sigma_y. \quad (2.11)$$

It is important if the detuning is small or large. This is because

$$\frac{\partial\alpha}{\partial x} = -\frac{k_L \frac{\delta_L}{\Omega} \sin[k_L(x - \Delta L \sin \omega t)]}{\left(\frac{\delta_L}{\Omega} \right)^2 + \cos^2[k_L(x - \Delta L \sin \omega t)]}; \quad \frac{\partial\alpha}{\partial t} = \frac{\omega \frac{\delta_L}{\Omega} \sin[k_L(x - \Delta L \sin \omega t)] \cos \omega t}{\left(\frac{\delta_L}{\Omega} \right)^2 + \cos^2[k_L(x - \Delta L \sin \omega t)]}. \quad (2.12)$$

So either for small or large detuning,

$$\delta_L \ll \Omega \quad \text{or} \quad \delta_L \gg \Omega \quad \Rightarrow \quad \frac{\partial\alpha}{\partial t}, \frac{\partial\alpha}{\partial x} \rightarrow 0. \quad (2.13)$$

2.1.1. Small detuning

Here, $\omega_0 \sim \omega_L$, thus $\tan \alpha \rightarrow \infty$ or $\alpha \sim \pi/2$. Considering equation (2.13) and keeping the terms up to $O(\hbar)$, the adiabatic Hamiltonian further simplifies to

$$H_{\text{ad},s}^{\text{RWA}} = \frac{p^2}{2m} \mathbf{I} + \hbar\Omega_{\text{eff}}\sigma_z. \quad (2.14)$$

Using the smallness of detuning, we may expand it binomially to obtain

$$H_{\text{ad},s}^{\text{RWA}, \pm} = \frac{p^2}{2m} \pm \frac{\hbar\Omega}{2} \cos[k_L(x - \Delta L \sin \omega t)] \left[1 + \frac{(\omega_0 - \omega_L)^2}{2\Omega^2 \cos^2[k_L(x - \Delta L \sin \omega t)]} \right] + \mathcal{O}\left(\left(\frac{\omega_0 - \omega_L}{\Omega} \right)^3 \right). \quad (2.15)$$

These provide the two PESs on which the two-level system evolves, connected by tunnelling. This can be seen by the fact that the intersection of the two curves occurs when Ω_{eff} is zero, leading to

²By classical correspondence, we assume the validity of Ehrenfest's theorem.

$$x = \Delta L \sin \omega t + \frac{\pi}{2k_L} + i \log \left(\sqrt{1 - \frac{\delta_L^2}{2\Omega^2}} - \frac{\delta_L}{\sqrt{2}\Omega} \right) \quad (2.16)$$

$$\simeq \Delta L \sin \omega t + \frac{\pi}{2k_L} - i \frac{\sqrt{2}\delta_L}{2\Omega},$$

for small detuning. The binding part of the potential in equation 2.15 supports eigenvalues. However, since the Hamiltonian is periodic in time, the eigenvalues are quasi-energies. Owing to the imaginary part, these are more precisely ‘quasi-energy resonances’.

2.1.2. Large detuning

We consider the case where we have the RWA and adiabatic approximation but $\delta_L \gg \Omega$. Then, we have the Hamiltonian,

$$H_{\text{ad},1}^{\text{RWA}} = \begin{pmatrix} p^2/2m + \hbar\Omega_{\text{eff}} & 0 \\ 0 & p^2/2m - \hbar\Omega_{\text{eff}} \end{pmatrix}. \quad (2.17)$$

This can be decomposed into two Hamiltonians

$$H_{\text{ad},1}^{\text{RWA}, \pm} = \frac{p^2}{2m} \pm \frac{\hbar\delta_L}{2} \left[1 + \frac{\Omega^2}{2\delta_L^2} \cos^2[k_L(x - \Delta L \sin \omega t)] \right] + \mathcal{O}\left(\left(\frac{\Omega}{\omega_0 - \omega_L}\right)^3\right). \quad (2.18)$$

The potential energy curves intersect when

$$x(t) = \left(n + \frac{1}{2}\right) \frac{\pi}{k_L} + \Delta L \sin \omega t. \quad (2.19)$$

Here, the intersection points are real where the real part is the same as for small detuning. The potential energy curves support sharp quasi-energies.

3. Exact solution

We now return to equation (1.6) and lift all the approximations considered in the last section. The Hamiltonian is written as

$$H_{\text{rot}} = \frac{p^2}{2m} \mathbf{I} + \begin{pmatrix} a & b \\ b^* & -a \end{pmatrix} \equiv \frac{p^2}{2m} \mathbf{I} + \mathcal{M}, \quad (3.1)$$

where $a = \hbar(\omega_0 - \omega_L)/2$, $b = b_1 + ib_2$, with

$$b_1 = \frac{\hbar\Omega}{2} \cos[k_L(x - \Delta L \sin \omega t)] (1 + \cos 2\omega_L t), \quad (3.2)$$

$$b_2 = -\frac{\hbar\Omega}{2} \cos[k_L(x - \Delta L \sin \omega t)] \sin 2\omega_L t.$$

The matrix denoted by \mathcal{M} in equation (3.1) can be diagonalized by matrix \mathcal{S} to get the diagonal matrix, \mathcal{J} . These matrices are

$$\mathcal{S} = \begin{pmatrix} \frac{(a - \sqrt{a^2 + b_1^2 + b_2^2})(b_1 + ib_2)}{b_1^2 + b_2^2} & \frac{(a + \sqrt{a^2 + b_1^2 + b_2^2})(b_1 + ib_2)}{b_1^2 + b_2^2} \\ 1 & 1 \end{pmatrix} \quad (3.3)$$

and

$$\mathcal{J} = \begin{pmatrix} -\sqrt{a^2 + b_1^2 + b_2^2} & 0 \\ 0 & \sqrt{a^2 + b_1^2 + b_2^2} \end{pmatrix}. \quad (3.4)$$

We define $\psi_1 = \mathcal{S}^{-1} \psi_{\text{rot}}$ with $i\hbar \partial \psi_{\text{rot}} / \partial t = \mathcal{H} \psi_{\text{rot}}$. The equation for the time evolution of ψ_1 is

$$i\hbar \frac{\partial \psi_1}{\partial t} = -i\mathcal{S}^{-1} \frac{\partial \mathcal{S}}{\partial t} \psi_1 + \mathcal{S}^{-1} \frac{p^2}{2m} \mathbf{I} \psi_1 + \mathcal{J} \psi_1. \quad (3.5)$$

Now, $\mathcal{S}^{-1}p^2\mathcal{S} = (\mathcal{S}^{-1}p\mathcal{S})^2 = (p - i\hbar\mathcal{S}^{-1}\partial\mathcal{S}/\partial x)^2$. Here, we again have a vector potential which is an artificial gauge field.

The Hamiltonian is thus written as an expansion [64,68]

$$H = H_0 + \hbar H_1 + \hbar^2 H_2 \quad (3.6)$$

with H_0 has a simple form

$$H_0 = \frac{p^2}{2m}\mathbf{I} + \begin{pmatrix} -\sqrt{a^2 + b_1^2 + b_2^2} & 0 \\ 0 & \sqrt{a^2 + b_1^2 + b_2^2} \end{pmatrix}. \quad (3.7)$$

Writing $\psi_1 = (\psi_1^{(+)} \ \psi_1^{(-)})^T$ with the superscript T denoting the transpose, we have written the state with two components. The classical Hamiltonians corresponding to the states, $\psi_1^{(\pm)}$ are

$$H_0^{(\pm)} = \frac{p^2}{2m} \pm \frac{\hbar(\omega_0 - \omega_L)}{2} \left(1 + \frac{4\Omega^2}{(\omega_0 - \omega_L)^2} \cos^2[k_L(x - \Delta L \sin \omega t)] \cos^2 \omega_L t \right)^{1/2}. \quad (3.8)$$

Usually, $\psi_1^{(+)}$ is subjected to a binding potential and $\psi_1^{(-)}$ is evolving on a scattering potential. There are two PESs, $\pm\sqrt{a^2 + b_1^2 + b_2^2}$ on which the full two-component wavefunction, ψ_1 , evolves. The PESs meet at the solution of

$$a^2 + b_1^2 + b_2^2 = 0. \quad (3.9)$$

The solution is

$$\begin{aligned} x &= \Delta L \sin \omega t + \frac{1}{k_L} \cos^{-1} \left[\pm i \frac{(\omega_0 - \omega_L)}{2\Omega} \sec(\omega_L t) \right] \\ &= \Delta L \sin \omega t + \frac{\pi}{2k_L} + i \frac{1}{k_L} \log \left[1 \mp \frac{\delta_L}{2\Omega} \sec(\omega_L t) + \frac{\delta_L^2}{8\Omega^2} \sec^2(\omega_L t) \right]. \end{aligned} \quad (3.10)$$

For small detuning ($\delta_L \ll \Omega$), the potential curves intersect at

$$x = \Delta L \sin \omega t + \frac{\pi}{2k_L} \mp i \frac{\delta_L}{2\Omega} \sec(\omega_L t) \pm i \frac{\delta_L^3}{48\Omega^3} \sec^3(\omega_L t). \quad (3.11)$$

The complex value of crossing the PESs implies the tunnelling of atoms. The tunnelling across these surfaces where the underlying dynamics is nonlinear has some very interesting related phenomena like resonance-assisted tunnelling [71], which have been recently experimentally realized [72].

Figure 1a,b shows these crossings along the complex position plane. We note that the crossing gap at the null imaginary position plane vanishes as one reaches closer to the resonance (at small detuning) and remains wide open at large detuning.

In equation (3.8), for large detuning, $\Omega^2/(\omega_0 - \omega_L)^2 \ll 1$, a Taylor expansion immediately yields

$$H_{0,l}^{(\pm)} = \frac{p^2}{2m} \pm \frac{\hbar(\omega_0 - \omega_L)}{2} \left(1 + \frac{2\Omega^2}{(\omega_0 - \omega_L)^2} \cos^2[k_L(x - \Delta L \sin \omega t)] \cos^2 \omega_L t \right). \quad (3.12)$$

Among the two Hamiltonians, $H_{0,l}^{(-)}$ is binding; it can be seen that the second term in the Taylor expansion of $\cos[k_L(x - \Delta L \sin \omega t)]$ along with an overall negative sign will make this roughly parabolic for small arguments, at least. For the same reason, $H_{0,l}^{(+)}$ is a scattering potential. The differences in Poincaré sections, obtained by slicing phase space evolution in the time intervals of the modulation period $T = 2\pi/\omega$ for various cases can be seen in figure 2a-d that are evaluated using numerical simulations (using Runge-Kutta order 4) for the classical equation of motions for Hamiltonians obtained from equations (3.8); (3.12); (2.17) and (2.18), respectively. We found that the three-island ring which is present in both unapproximated case and RWA + Adiabatic case vanishes if we make a binomial approximation implying that the origin of this resonance is purely arising because of higher order terms of equations (3.12) and (2.15). We also note that the chaos is more apparent in the binomial case but less severe in all other cases.

We now study the classical mechanics of these Hamiltonians.

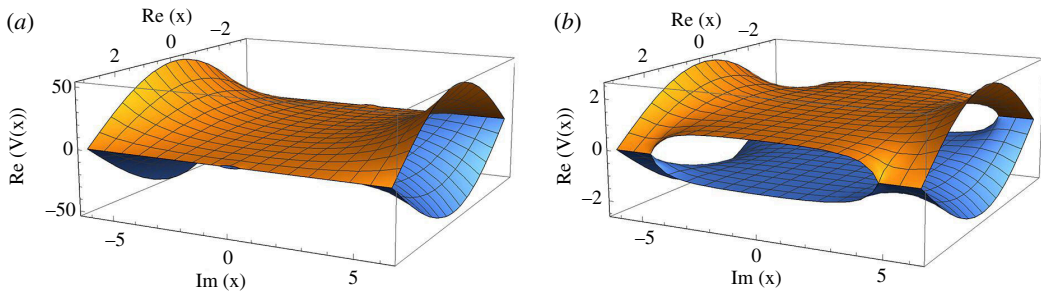


Figure 1. PES at (a) large detuning ($\delta_L \gg \Omega$) and (b) small detuning ($\delta_L \ll \Omega$). At large detuning, the gap shrinks allowing a larger region for space for crossing the PES.

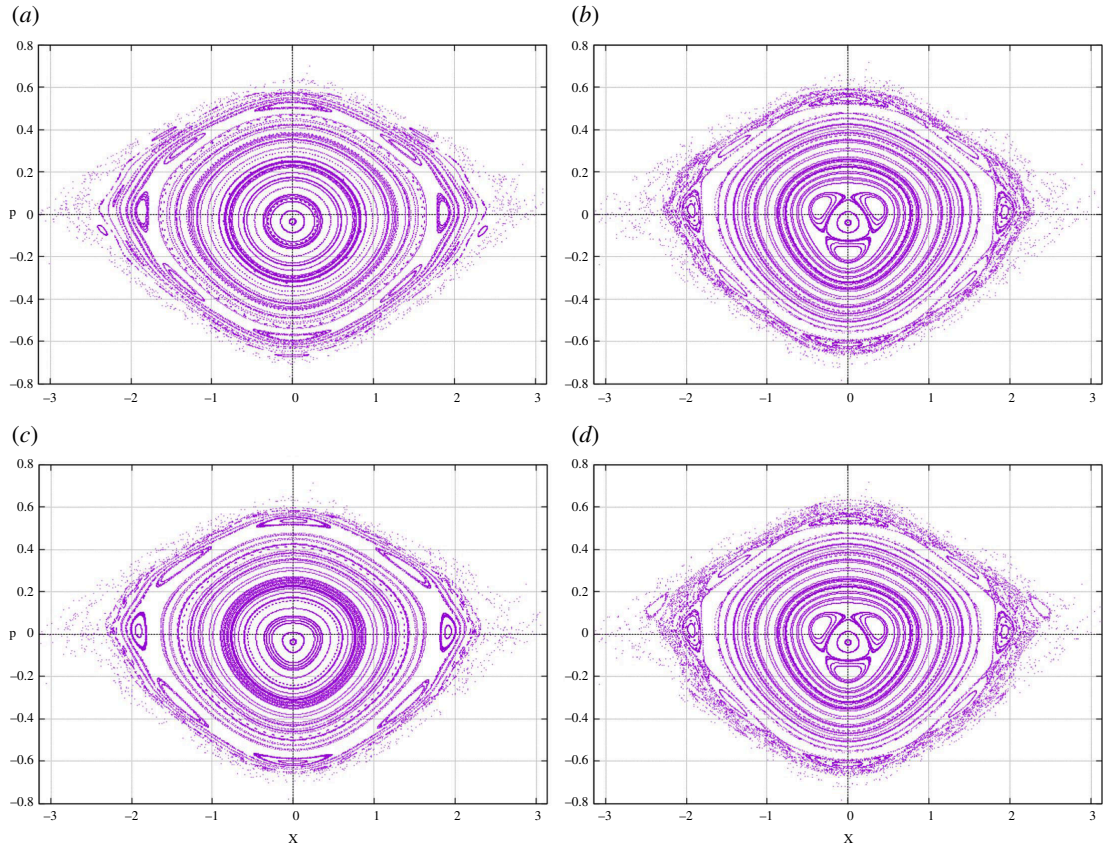


Figure 2. Comparison of Poincaré sections for Hamiltonians under different approximations for the case of large detuning for the same set of parameters used in figure 3. (a) Shows the unapproximated case corresponding to the exact solution. (b) Shows the application of binomial approximation to the exact solution. (c) Corresponds to the RWA + Adiabatic approximation and (d) corresponds to the RWA + Adiabatic + Binomial approximation. Initial conditions and number of evolution steps are kept the same for all cases here.

4. Quasi-integrability

In this section, we study the classical dynamics of the Hamiltonians obtained above under different approximations.

We begin with the exact Hamiltonian, namely, equation (3.6) and consider only $H_0^{(-)}$ in equation (3.8). We make the following transformations to convert it to a dimensionless form almost similar to [63]:

$$\begin{aligned}
 t &\rightarrow \frac{t}{\omega}, \quad x \rightarrow \frac{x}{2k_L}, \quad p \rightarrow \frac{M\omega p}{2k_L}, \quad H_0 \rightarrow \frac{M\omega^2 H_0}{4K_L^2} \\
 \lambda &= 2k_L \Delta L, \quad \gamma = \frac{\omega_L}{\omega}, \quad \eta = \left(\frac{\Omega}{\delta_L}\right)^2, \quad K = \frac{\hbar k_L^2 \Omega^2}{2M\omega^2 \delta_L}
 \end{aligned}
 \tag{4.1}$$

where η is the strength of Rabi resonance and $\delta_L = \omega_0 - \omega_L$ is the detuning of laser. The simplified Hamiltonian yields

$$H_0 = \frac{p^2}{2} - \frac{4K}{\eta} [1 + 2\eta(1 + \cos(x - \lambda \sin t)) \cos^2 \gamma t]^{\frac{1}{2}}. \quad (4.2)$$

Now, using the same transformations (equation (4.1)), we write the Hamiltonians for large detuning, neglecting the constant terms,

$$H_{0,l} \simeq \frac{p^2}{2} - 4K \cos(x - \lambda \sin t) \cos^2 \gamma t, \quad (4.3)$$

$$H_{\text{ad},1}^{\text{RWA},-} \simeq \frac{p^2}{2} - K \cos(x - \lambda \sin t). \quad (4.4)$$

This clearly implies a drastic change in the equation if $\gamma \gg 1$, thus even if we use $\langle \cos^2 \gamma t \rangle = 1/2$, the second term contributes to double compared with the contribution coming from the usual case with adiabatic and RWA.

In order to understand the underlying phase space structure, we initialize 1000 ultracold atoms (purple dots) in one of the islands in the Poincarè section taken in steps of modulation time period T as shown in figure 3a and look at its stroboscopic evolution in multiples of the modulation time period. We found that after each modulation period, atoms move from one island to another lying around the same larger elliptic-like orbit (figure 3b). Similarly, we found that the number of islands is equal to (or twice if n is even) the number of modulation periods n for the marked islands in figure 3c. In other words, these islands satisfy $T_{\text{orbit}} = nT$ or $\Omega_{\text{orbit}}/\omega = 1/n$.

To study the origin of these patterns in resonance structures, we write the dimensionless Hamiltonian equation (4.4) in action-angle variables. Let us write one of the RWA Hamiltonians as a perturbed harmonic oscillator

$$H_{0,l}^{\text{RWA},-} = \frac{p^2}{2} + \frac{Kx^2}{2} - \left(K \cos(x - \lambda \sin t) + \frac{Kx^2}{2} \right), \quad (4.5)$$

$$= H_{\text{h.o.}} + \epsilon \Delta H, \quad (4.6)$$

where ϵ is introduced for book keeping (eventually, we shall put $\epsilon = 1$). Using the oscillator action-angle variables, (J, θ) , with $x = \sqrt{\frac{J}{\pi\Omega}} \sin(\theta)$ and $p = \sqrt{\frac{J\Omega}{\pi}} \cos(\theta)$ with $K = \Omega^2$, the Hamiltonians are

$$H_{\text{h.o.}} = \frac{\Omega J}{2\pi}, \quad (4.7)$$

$$\Delta H = -\Omega^2 \cos\left(\sqrt{\frac{J}{\pi\Omega}} \sin \theta - \lambda \sin t\right) - \frac{J\Omega}{2\pi} \sin^2 \theta. \quad (4.8)$$

We use the classical time-dependent perturbation theory [59] to calculate the associated action of this Hamiltonian up to first order in perturbation. For this, we transform the action variables in a way that the new Hamiltonian \bar{H} is only a function of the new action variable \bar{J} alone. We obtain

$$\langle \Delta H \rangle = \frac{1}{2\pi} \int_0^{2\pi} dt \frac{1}{2\pi} \int_0^{2\pi} d\theta \Delta H(J, \theta, t) \quad (4.9)$$

$$= -\Omega^2 J_0\left(\sqrt{\frac{\bar{J}}{\Omega\pi}}\right) J_0(\lambda) - \frac{\bar{J}\Omega}{4\pi}$$

$$\bar{H}(\bar{J}) = \frac{\Omega \bar{J}}{2\pi} - \epsilon \Omega^2 J_0\left(\sqrt{\frac{\bar{J}}{\Omega\pi}}\right) J_0(\lambda) - \epsilon \frac{\bar{J}\Omega}{4\pi} \quad (4.10)$$

where $J_0(\cdot)$ is the cylindrical Bessel function of order zero. The new frequency is

$$\Omega'(\bar{J}) = 2\pi \frac{\partial \bar{H}}{\partial \bar{J}} = \Omega(1 - \epsilon/2) - 2\epsilon\pi\Omega^2 J_0'\left(\sqrt{\frac{\bar{J}}{\Omega\pi}}\right) J_0(\lambda) \quad (4.11)$$

where prime on the Bessel function denotes a derivative with respect to its argument.

We subtract this $\epsilon \langle \Delta H \rangle$ from $\epsilon \Delta H$ to obtain the oscillating part $\epsilon \{ \Delta H \}$. For calculating the integral, we expand the potential term using Jacobi–Anger expansion [73] $e^{iz \sin \theta} = \sum_{n=-\infty}^{+\infty} J_n(z) e^{in\theta}$.

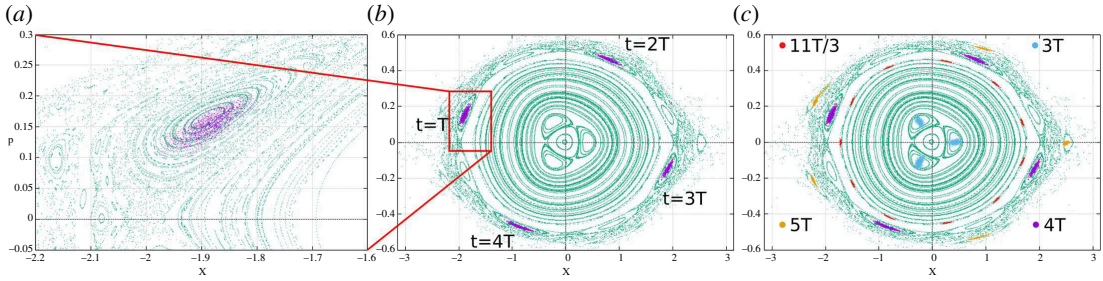


Figure 3. Poincaré sections taken in steps of the modulation period using the same parameter as in [1]. (a) 1000 ultracold atoms (purple dots) are loaded in one of the islands of stability in the Poincaré section taken in steps of the driving period T . (b) Stroboscopic evolution of the ultracold atoms reveals that they evolve with period $4T$. (c) Similarly, loading on different islands of stability shows the existence of $3T$, $11T/3$, $4T$ and $5T$ periods predominantly.

$$\{\Delta H\} = - \sum_{n,m=-\infty}^{\infty} \Omega^2 J_n \left(\sqrt{\frac{\bar{J}}{\Omega\pi}} \right) J_m(\lambda) \cos(n\bar{\theta} - mt) + \frac{\bar{J}\Omega}{4\pi} \cos 2\bar{\theta} \quad (4.12)$$

$$\equiv \sum_{n,m=-\infty}^{\infty} \Delta H_{n,m}(\bar{J}, \bar{\theta}, t) + \frac{\bar{J}\Omega}{4\pi} \cos 2\bar{\theta}, \quad (4.13)$$

where both n, m are non-zero. The change in action $\epsilon\Delta S$ can be calculated as

$$\epsilon\Delta S = - \int^t dt \epsilon\{\Delta H\} \quad (4.14)$$

$$= \sum_{n,m=-\infty}^{\infty} \epsilon\Delta S_{n,m}(\bar{J}, \bar{\theta}, t) + \frac{\epsilon\bar{J}\Omega}{8\pi\bar{\Omega}(J)} \sin 2\bar{\theta}, \quad (4.15)$$

where

$$\epsilon\Delta S_{n,m} = \frac{-\epsilon\Omega^2}{n\bar{\Omega}(\bar{J}) - m} J_n \left(\sqrt{\frac{\bar{J}}{\Omega\pi}} \right) J_m(\lambda) \sin(n\bar{\theta} - mt). \quad (4.16)$$

Consequent to the above,

$$\bar{J} = J - \epsilon \frac{\partial \Delta S}{\partial \theta}(J, \theta, t); \quad \bar{\theta} = \theta + \epsilon \frac{\partial \Delta S}{\partial J}(J, \theta, t). \quad (4.17)$$

The new action-angle variables can be calculated up to first order as

$$\bar{J} = J + \epsilon \frac{n\Omega^2}{n\bar{\Omega}(J) - m} J_n \left(\sqrt{\frac{J}{\Omega\pi}} \right) J_m(\lambda) \cos(n\theta - mt) - \epsilon \frac{J\Omega}{4\pi} \cos 2\theta, \quad (4.18)$$

$$\bar{\theta} = \theta + \epsilon \frac{-\Omega^2}{n\bar{\Omega}(J) - m} J_n' \left(\sqrt{\frac{J}{\Omega\pi}} \right) J_m(\lambda) \sin(n\theta - mt) + \frac{\epsilon\Omega}{8\pi\bar{\Omega}(J)} \sin 2\theta. \quad (4.19)$$

Thus, we have obtained the action with resonant denominators which leads to the resonant condition

$$n\bar{\Omega}(\bar{J}) = m\omega, \quad (4.20)$$

where ω is the modulation frequency and $\bar{\Omega}(\bar{J})$ is the frequency of the orbit; ω is obtained when we substitute the actual time, t , in place of dimensionless time from equation (4.1). This explains the observed pattern in figure 3: the orbital periods are the integral multiples of the modulation period at the resonance. The strength of (n, m) th resonance is determined by the product of two Bessel functions $J_n(\sqrt{J/\Omega\pi})$ and $J_m(\lambda)$. Using the first-order correction in the frequency $\Omega(J)$, we plot it as a function of J in figure 4. We see that only the 1:3 resonance is allowed under first-order correction. This means that all other resonances in figure 3 must originate from the higher-order perturbation terms in correction for $\bar{\Omega}$ and \bar{J} . That explains the dominance of primary islands in $(n, m)=(3, 1)$ resonance and the presence of secondary islands in other resonances.

For the expression without binomial approximation equation (4.4), where in figure 2, we saw (3,1) resonance to be dominantly present, but without binomial approximation (equation 2.17), this resonance is suppressed and does not appear. This can lead to significant corrections for both quantum and classical equations despite being in a large detuning limit. Similarly, very high-ordered resonances

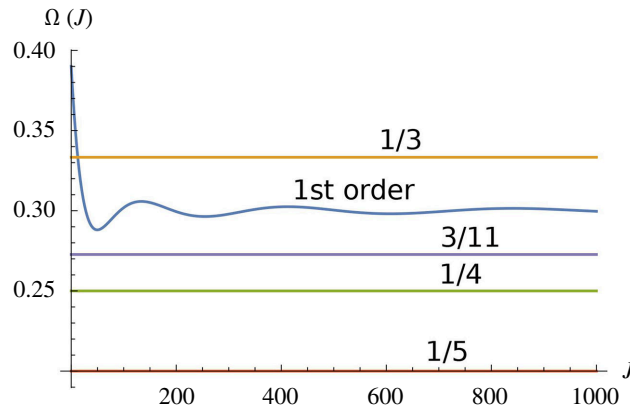


Figure 4. First order correction in $\Omega(J)$. Only those resonances whose frequency ratio $\Omega(J):\omega$ ($\omega=1$ here) intersect with $\Omega(J)$ are allowed.

are enhanced by binomial approximation as the chaotic regime can be seen enhanced around the edges for this case.

5. Dynamical localization

Let us imagine that we prepare the initial state of the atoms as a localized wavepacket. As the system evolves, the wavepacket spreads. The wavefunction of the two-state system is shown to evolve, in all versions of description, on a pair of PESs. The form of these potentials readily supports the bounded dynamics of one of the potentials. The complex intersection points provide paths for tunnelling. The succession of these two dynamical features leads to the localization of the wavepacket. The physics of this is nothing but the well-known argument by Mott & Twose [74] and Anderson [54], adapted in recent times in quantum chaos [55,56].

6. Conclusions

When a collection of atoms is subjected to phase modulation, the quantum and classical dynamics are dictated by several frequencies. The quantum dynamics of the two-level systems has been studied in the past where the main result was the observation of dynamical localization by Raizen's group [1]. The theoretical analysis of the system has been carried out under various approximations and discussed at a didactic level [63]. Here, we perform the analysis of this system by using successive unitary transformations on the off-diagonal part of the Hamiltonian in the process of diagonalization, as explained in §3. We have worked with the transformed Hamiltonian which is diagonal to $O(1)$. Our analysis, following earlier works in chemical physics and nuclear physics, explained in detail in a comprehensive review [64], shows that the dynamics of the two-state system take place on coupled PESs. The connection between the two surfaces occurs via tunnelling and the underlying classical dynamics is shown to be quasi-integrable of the KAM type. This is brought out by the Poincaré surfaces of sections where we note the presence of elliptic and hyperbolic points, typically paraphrased as dynamics occurs in the mixed-phase space with 'stable islands in the stochastic sea'. A detailed understanding of dynamics is interesting and illuminating.

Let us comment about the usage of the term 'exact'. Upon diagonalization of the potential matrix, there appears a 'vector potential' in the kinetic energy term, leading to terms in orders of Planck's constant. The transformed Hamiltonian is $[(\mathbf{p} - \hbar\mathbf{A})^2/2 + \mathbf{v}]$. The important point is that $(p^2/2m + v)\mathbf{I}$ is diagonal whereas the other terms of orders \hbar and \hbar^2 are not diagonal. Our objective is to diagonalize the Hamiltonian matrix. At this step, the diagonalization is up to $O(1)$. This process can be repeated by diagonalizing the off-diagonal terms in $\mathbf{A}\cdot\mathbf{p}$ and $\mathbf{A}\cdot\mathbf{A}$ by successive unitary transformations. In principle, this process can be repeated ad infinitum, leading to complete diagonalization.

The approximated analysis has certain appeal insofar as tunnelling between islands is seen clearly. However, to establish the existence of islands and tunnelling, we show that the onset of islands of stability can be seen from the first-order perturbation theory.

As explained above, the analysis reveals a vector potential that is related to an artificial gauge field. We believe that knowing the form of this could be useful for experiments with cold atoms and in developing the fields of Hamiltonian engineering, quantum sensing and quantum interference. We have not developed these aspects here.

As referred to in the Introduction, our results add to the discussion of integrability in matrix models for atomic systems, in particular to the work on the quantum Rabi model [61]. In the future, by adding nonlinear terms to incorporate interactions that allow the control of atomic states, these works could be useful for critical quantum metrology [75]. The control of states of multi-qubit systems [76] and their protection [77] belongs to the present theme in a rather compelling manner.

Ethics. This work did not require ethical approval from a human subject or animal welfare committee.

Data accessibility. This article has no additional data.

Declaration of AI use. We have not used AI-assisted technologies in creating this article.

Authors' contributions. R.G.: conceptualization, data curation, formal analysis, investigation, methodology, software, validation, visualization, writing—original draft, writing—review and editing; M.J.: conceptualization, data curation, formal analysis, investigation, methodology, software, validation, visualization, writing—original draft, writing—review and editing; S.R.J.: Conceptualization, data curation, formal analysis, investigation, methodology, software, supervision, validation, visualization, writing—original draft, writing—review and editing.

All authors gave final approval for publication and agreed to be held accountable for the work performed therein.

Conflict of interest declaration. We declare we have no competing interests.

Funding. No funding has been received for this article.

Acknowledgements. We thank Sandeep Joshi for several helpful discussions. R.G. acknowledges the fellowship support received from CSIR-HRDG.

References

- Moore F, Robinson J, Bharucha C, Williams P, Raizen M. 1994 Observation of dynamical localization in atomic momentum transfer: a new testing ground for quantum chaos. *Phys. Rev. Lett.* **73**, 2974–2977. (doi:10.1103/PhysRevLett.73.2974)
- Thalhammer G, Barontini G, De Sarlo L, Catani J, Minardi F, Inguscio M. 2008 Double species Bose–Einstein condensate with tunable interspecies interactions. *Phys. Rev. Lett.* **100**, 210402. (doi:10.1103/PhysRevLett.100.210402)
- Cui Y, Deng M, You L, Gao B, Tey MK. 2018 Broad Feshbach resonances in ultracold alkali–metal systems. *Phys. Rev. A.* **98**, 042708. (doi:10.1103/PhysRevA.98.042708)
- Lamporesi G, Catani J, Barontini G, Nishida Y, Inguscio M, Minardi F. 2010 Scattering in mixed dimensions with ultracold gases. *Phys. Rev. Lett.* **104**, 153202. (doi:10.1103/PhysRevLett.104.153202)
- Tanzi L, Cabrera CR, Sanz J, Cheiney P, Tomza M, Tarruell L. 2018 Feshbach resonances in potassium Bose–Bose mixtures. *Phys. Rev. A.* **98**, 062712. (doi:10.1103/PhysRevA.98.062712)
- D'Errico C, Zaccanti M, Fattori M, Roati G, Inguscio M, Modugno G, Simoni A. 2007 Feshbach resonances in ultracold ³⁹K. *New J. Phys.* **9**, 223. (doi:10.1088/1367-2630/9/7/223)
- Marte A, Volz T, Schuster J, Dürr S, Rempe G, van Kempen EGM, Verhaar BJ. 2002 Feshbach resonances in rubidium 87: precision measurement and analysis. *Phys. Rev. Lett.* **89**, 283202. (doi:10.1103/PhysRevLett.89.283202)
- Yurovsky VA, Ben-Reuven A. 2003 Three-body loss of trapped ultracold ⁸⁷Rb atoms due to a Feshbach resonance. *Phys. Rev. A.* **67**, 050701. (doi:10.1103/PhysRevA.67.050701)
- Vogels JM, Tsai CC, Freeland RS, Kokkelmans SJJMF, Verhaar BJ, Heinzen DJ. 1997 Prediction of Feshbach resonances in collisions of ultracold rubidium atoms. *Phys. Rev. A.* **56**, R1067–R1070. (doi:10.1103/PhysRevA.56.R1067)
- Blackley CL, Le Sueur CR, Hutson JM, Hung-Wen C, Jenkin DL, Cornish SL. 2013 Feshbach resonances in ultracold ⁸⁵Rb. *Phys. Rev. A.* **87**, 033611. (doi:10.1103/PhysRevA.87.033611)
- Tobias F, Alexander G, Wilson KE, Jack S, Frye MD, Hutson JM, Cornish SL. 2022 Observation of magnetic Feshbach resonances between Cs and ¹⁷³Yb. *Phys. Rev. Res.* **4**, 043072. (doi:10.1103/PhysRevResearch.4.043072)
- Hung-Wen C, et al. 2013 Feshbach spectroscopy of an ultracold mixture of ⁸⁵Rb and ¹³³Cs. *Phys. Rev. A.* **87**, 010703. (doi:10.1103/PhysRevA.87.010703)
- Catani J, De Sarlo L, Barontini G, Minardi F, Inguscio M. 2008 Degenerate Bose–Bose mixture in a three-dimensional optical lattice. *Phys. Rev. A.* **77**, 011603. (doi:10.1103/PhysRevA.77.011603)
- Wacker LJ, Jørgensen NB, Birkmose D, Winter N, Mikkelsen M, Sherson J, Zinner N, Arlt JJ. 2016 Universal three-body physics in ultracold KRb mixtures. *Phys. Rev. Lett.* **117**, 163201. (doi:10.1103/PhysRevLett.117.163201)
- Ferrari G, Inguscio M, Jastrzebski W, Modugno G, Roati G, Simoni A. 2002 Collisional properties of ultracold K–Rb mixtures. *Phys. Rev. Lett.* **89**, 053202. (doi:10.1103/PhysRevLett.89.053202)

16. Sawant R, Maffei A, Barontini G. 2021 Thermalization of a trapped single atom with an atomic thermal bath. *Appl. Sci.* **11**, 2258. (doi:10.3390/app11052258)
17. Mosk A, Kraft S, Mudrich M, Singer K, Wohlleben W, Grimm R, Weidemüller M. 2001 Mixture of ultracold lithium and cesium atoms in an optical dipole trap. *Appl. Phys. B.* **73**, 791–799. (doi:10.1007/s003400100743)
18. Hewitt T, Bertheas T, Jain M, Nishida Y, Barontini G. 2023 Controlling the interactions in a cold atom quantum impurity system. *arXiv*. See <https://arxiv.org/abs/2310.02771>
19. Kasevich M, Chu S. 1991 Atomic interferometry using stimulated Raman transitions. *Phys. Rev. Lett.* **67**, 181–184. (doi:10.1103/PhysRevLett.67.181)
20. Rosi G *et al.* 2018 Detecting gravitational waves with atomic sensors. *Nuovo Cimento Della Società Italiana Di Fisica C, Geophys. Space Phys.* **41**, 130. (doi:10.1393/ncc/i2018-18130-8)
21. Rosi G. 2017 A proposed atom interferometry determination of G at 10^{-5} using a cold atomic fountain. *Metrologia* **55**, 50. (doi:10.1088/1681-7575/aa8fd8)
22. Rosi G, Sorrentino F, Cacciapuoli L, Prevedelli M, Tino GM. 2014 Precision measurement of the Newtonian gravitational constant using cold atoms. *Nature* **510**, 518–521. (doi:10.1038/nature13433)
23. Rosi G, D'Amico G, Cacciapuoli L, Sorrentino F, Prevedelli M, Zych M, Brukner Č, Tino GM. 2017 Quantum test of the equivalence principle for atoms in coherent superposition of internal energy states. *Nat. Commun.* **8**, 15529. (doi:10.1038/ncomms15529)
24. Jain M, Tino GM, Cacciapuoli L, Rosi G. 2022 Reply to comment on “New apparatus design for high precision measurement of G with atom interferometry.” *Eur. Phys. J. D.* **76**, 164. (doi:10.1140/epjd/s10053-022-00489-1)
25. Jain M, Tino GM, Cacciapuoli L, Rosi G. 2021 New apparatus design for high-precision measurement of G with atom interferometry. *Eur. Phys. J. D.* **75**, 197. (doi:10.1140/epjd/s10053-021-00212-6)
26. D'Amico G, Cacciapuoli L, Jain M, Zhan S, Rosi G. 2019 Measuring the gravitational acceleration with matter-wave velocimetry. *Eur. Phys. J. D.* **73**, 98. (doi:10.1140/epjd/e2019-90543-0)
27. Tino GM, Salvi L, Cacciapuoli L, D'Amico G, Hu L, Jain M, Poli N, Rosi G, Wang E. 2018 Testing gravity with atomic quantum sensors on ground and in space. In *Proc. SPIE 10674, Quantum Technologies 2018, Strasbourg, France*, **10674**, pp.1067409. (doi:10.1117/12.2317923)
28. Tino GM. 2021 Testing gravity with cold atom interferometry: results and prospects. *Quantum Sci. Technol.* **6**, 024014. (doi:10.1088/2058-9565/abd83e)
29. Lamporesi G, Bertoldi A, Cacciapuoli L, Prevedelli M, Tino GM. 2008 Determination of the Newtonian gravitational constant using atom interferometry. *Phys. Rev. Lett.* **100**, 050801. (doi:10.1103/PhysRevLett.100.050801)
30. Liu J, Wang X, Mellado Muñoz J, Kowalczyk A, Barontini G. 2019 Vortex conveyor belt for matter-wave coherent splitting and interferometry. *Sci. Rep.* **9**, 1267. (doi:10.1038/s41598-019-38641-4)
31. Canuel B *et al.* 2006 Six-axis inertial sensor using cold-atom interferometry. *Phys. Rev. Lett.* **97**, 010402. (doi:10.1103/PhysRevLett.97.010402)
32. Aguilera DN *et al.* 2014 STE-QUEST—test of the universality of free fall using cold atom interferometry. *Class. Quantum Grav.* **31**, 115010. (doi:10.1088/0264-9381/31/11/115010)
33. Biedermann GW, Wu X, Deslauriers L, Roy S, Mahadeswaraswamy C, Kasevich MA. 2015 Testing gravity with cold-atom interferometers. *Phys. Rev. A.* **91**, 033629. (doi:10.1103/PhysRevA.91.033629)
34. Kale YB, Singh A, Gellesch M, Jones JM, Morris D, Aldous M, Bongs K, Singh Y. 2022 Field deployable atomics package for an optical lattice clock. *Quantum Sci. Technol.* **7**, 045004. (doi:10.1088/2058-9565/ac7b40)
35. Qiushuo S *et al.* 2023 *Frequency & time: measurements, control and transfer*, **1**. IFSA Publishing. See https://www.sensorsportal.com/HTML/Frequency_and_Time_Vol_2.htm
36. Ludlow AD, Boyd MM, Ye J, Peik E, Schmidt PO. 2015 Optical atomic clocks. *Rev. Mod. Phys.* **87**, 637–701. (doi:10.1103/RevModPhys.87.637)
37. Barontini G *et al.* 2022 Measuring the stability of fundamental constants with a network of clocks. *EPL Quantum Technol.* **9**, 12. (doi:10.1140/epjqt/s40507-022-00130-5)
38. Masao T, Feng-Lei H, RyoichiH, HidetoshiK. 2005 An optical lattice clock. *Nature* **435**, 321. (doi:10.1038/nature03541)
39. Bordé CJ. 2002 Atomic clocks and inertial sensors. *Metrologia* **39**, 435–463. (doi:10.1088/0026-1394/39/5/5)
40. Ichiro U, Masao T, Manoj D, TakuyaO, Hidetoshi K. 2015 Cryogenic optical lattice clocks. *Nat. Photon* **9**, 185. (doi:10.1038/nphoton.2015.5)
41. Andrei D, Hidetoshi K. 2011 Colloquium: physics of optical lattice clocks. *Rev. Mod. Phys.* **83**, 331. (doi:10.1103/RevModPhys.83.331)
42. Yamanaka K, Ohmae N, Ushijima I, Takamoto M, Katori H. 2015 Frequency ratio of ^{199}Hg and ^{87}Sr optical lattice clocks beyond the SI limit. *Phys. Rev. Lett.* **114**, 230801. (doi:10.1103/PhysRevLett.114.230801)
43. Zheng X, Dolde J, Lochab V, Merriman BN, Li H, Kolkowitz S. 2022 Differential clock comparisons with a multiplexed optical lattice clock. *Nature* **602**, 425–430. (doi:10.1038/s41586-021-04344-y)
44. Nicola P, Oates CW, Patrick G, Tino GM. 2013 Optical atomic clocks. *La Rivista Del Nuovo Cimento.* **36**, 555. (doi:10.1393/nrc/i2013-10095-x)
45. Zhang W, Walls DF. 1993 Quantum diffraction of ultracold atoms by a standing wave laser. *Quantum Opt.* **5**, 9–14. (doi:10.1088/0954-8998/5/1/002)
46. Jain M. 2018 Classical system underlying a diffracting quantum billiard. *Pramana - J. Phys.* **90**, 20. (doi:10.1007/s12043-017-1509-6)
47. Barontini G, Paternostro M. 2019 Ultra-cold single-atom quantum heat engines. *New J. Phys.* **21**, 063019. (doi:10.1088/1367-2630/ab2684)
48. Muñoz JM, Wang X, Hewitt T, Kowalczyk AU, Sawant R, Barontini G. 2020 Dissipative distillation of supercritical quantum gases. *Phys. Rev. Lett* **125**, 020403. (doi:10.1103/PhysRevLett.125.020403)

49. Glatthard J, Rubio J, Sawant R, Hewitt T, Barontini G, Correa LA. 2022 Optimal cold atom thermometry using adaptive Bayesian strategies. *PRX Quantum*. **3**, 040330. (doi:10.1103/PRXQuantum.3.040330)
50. Vogler A, Labouvie R, Stubenrauch F, Barontini G, Guarrera V, Ott H. 2013 Thermodynamics of strongly correlated one-dimensional Bose gases. *Phys. Rev. A*. **88**. (doi:10.1103/PhysRevA.88.031603)
51. Softley TP. 2023 Cold and ultracold molecules in the twenties. *Proc. R. Soc. A*. **479**, 20220806. (doi:10.1098/rspa.2022.0806)
52. Singh V. 2021 Theoretical investigation of a two-stage buffer gas cooled beam source. *Cryogenics* **118**, 103335. (doi:10.1016/j.cryogenics.2021.103335)
53. Ozawa T, Price HM. 2019 Topological quantum matter in synthetic dimensions. *Nat. Rev. Phys.* **1**, 349–357. (doi:10.1038/s42254-019-0045-3)
54. Anderson PW. 1958 Absence of diffusion in certain random lattices. *Phys. Rev.* **109**, 1492–1505. (doi:10.1103/PhysRev.109.1492)
55. Fishman S, Grepel DR, Prange RE. 1982 Chaos, quantum recurrences, and Anderson localization. *Phys. Rev. Lett.* **49**, 509–512. (doi:10.1103/PhysRevLett.49.509)
56. Jain SR. 1993 Fractal-like quasienergy spectrum in the Fermi-Ulam model. *Phys. Rev. Lett.* **70**, 3553–3556. (doi:10.1103/PhysRevLett.70.3553)
57. Billy J et al. 2008 Direct observation of Anderson localization of matter waves in a controlled disorder. *Nature* **453**, 891–894. (doi:10.1038/nature07000)
58. Graham R, Schlautmann M, Zoller P. 1992 Dynamical localization of atomic-beam deflection by a modulated standing light wave. *Phys. Rev. A*. **45**, R19–R22. (doi:10.1103/physreva.45.r19)
59. Lichtenberg AJ, Leiberman MA. 1992 *Regular and chaotic dynamics*. New York, NY: Springer. See <http://link.springer.com/10.1007/978-1-4757-2184-3>
60. Berry MV. 1978 Regular and irregular motion. *AIP Conference Proceedings*, Vol. 46, 16–120. (doi:10.1063/1.31417)
61. Braak D. 2011 Integrability of the Rabi model. *Phys. Rev. Lett.* **107**, 100401. (doi:10.1103/PhysRevLett.107.100401)
62. Braak D. 2019 Symmetries in the quantum Rabi model. *Symmetry* **11**, 1259. (doi:10.3390/sym11101259)
63. Stöckmann HJ. 1999 Quantum chaos. *Quantum chaos: an introduction*. Cambridge, UK: Cambridge University Press. (doi:10.1017/CB09780511524622)
64. Gaspard P, Alonso D, Burghardt I. 1995 New ways of understanding semiclassical quantization. *Adv. Chem. Phys.* **90**, 105. (doi:10.1002/9780470141496)
65. Voros A. 1977 Asymptotic -expansions of stationary quantum states.[Bohr-Sommerfeld formula]. *Ann. Inst. Henri Poincaré, Sect. A;(France)* **26**, 343–403. See http://www.numdam.org/article/AIHPA_1977__26_4_343_0.pdf
66. Keller JB. 1985 Semiclassical mechanics. *SIAM Rev.* **27**, 485–504. (doi:10.1137/1027139)
67. Gaspard P, Alonso D. 1993 \hbar expansion for the periodic-orbit quantization of hyperbolic systems. *Phys. Rev. A*. **47**, R3468–R3471. (doi:10.1103/physreva.47.r3468)
68. Jain SR. 2004 Semiclassical deuteron. *J. Phys. G: Nucl. Part. Phys.* **30**, 157–164. (doi:10.1088/0954-3899/30/2/013)
69. Dwivedi NR, Kaur H, Jain SR. 2018 Semiclassical triton. *Eur. Phys. J. A*. **54**, 49. (doi:10.1140/epja/i2018-12480-y)
70. Brack M, Jain SR. 1995 Analytical tests of Gutzwiller's trace formula for harmonic-oscillator potentials. *Phys. Rev. A*. **51**, 3462–3468. (doi:10.1103/physreva.51.3462)
71. Brodier O, Schlagheck P, Ullmo D. 2002 Resonance-assisted tunneling. *Ann. Phys.* **300**, 88–136. (doi:10.1006/aphy.2002.6281)
72. Gehler S, Löck S, Shinohara S, Bäcker A, Ketzmerick R, Kuhl U, Stöckmann HJ. 2015 Experimental observation of resonance-assisted tunneling. *Phys. Rev. Lett.* **115**, 104101. (doi:10.1103/PhysRevLett.115.104101)
73. Abramowitz M, Stegun I. 1965 *Handbook of mathematical functions with formulas, graphs, and mathematical tables*. Mineola, NY: Dover Publications. See <https://dl.acm.org/doi/10.5555/1098650>
74. Mott NF, Twose WD. 1961 The theory of impurity conduction. *Adv. Phys.* **10**, 107–163. (doi:10.1080/00018736100101271)
75. Ying ZJ, Felicetti S, Liu G, Braak D. 2022 Critical quantum metrology in the non-linear quantum Rabi model. *Entropy*. **24**, 1015. (doi:10.3390/e24081015)
76. Kumari K, Rajpoot G, Joshi S, Jain SR. 2023 Qubit control using quantum Zeno effect: action principle approach. *Ann. Phys.* **450**, 169222. (doi:10.1016/j.aop.2023.169222)
77. Saini RK, Sehgal R, Jain SR. 2022 Protection of qubits by nonlinear resonances. *Eur. Phys. J. Plus*. **137**, 356. (doi:10.1140/epjp/s13360-022-02561-6)